Development of a phenomenological equation to predict tool wear in friction stir welding by steel grades in Al/Steel lap joining

Tremblay, F.; Nadeau, F.; St-Georges, L.

Publisher's version / Version de l'éditeur:

Proceedings of the 12th International Symposium on FSW, 2018-06

Development of a phenomenological equation to predict tool wear in friction stir welding by steel grades in Al/Steel lap joining

F. Tremblay – NRC; F. Nadeau – NRC; L. St-Georges – UQAC;

INTRODUCTION

Since its introduction in the industry, the amount of structures being joined by friction stir welding (FSW) are in progression [1]. Even if low-melting point materials such as aluminium or magnesium represents the highest number of applications, this method can also successfully join materials with different melting point as in the case of aluminium to steel. As lightweigthing structures gained ground in the last few years and will still continue to grow, joining processes combining aluminium to steel effectively need to be developed further [2].

When it comes down to join aluminium to steel, the most common configuration is lap joint which the FSW pin enters into the bottom sheet substrate, thus the steel material. In order to have a FSW tool that lasts a sufficient amount of time, the material needs to sustain high stresses and temperatures and still be affordable, such as WC-based tools [3, 4]. The wear rate of the tool used during the process needs to be known and understood as it dictates the applicability of the FSW method depending of the application. As an example, the sub-frame assembly of the Honda Accord 2013 is joined using aluminium to steel FSW lap joining [5].

Be able to predict when the tool reaches a point where it is no longer effective to produce a sound weld can certainly help to evaluate tool life. Actually, a few papers have produced a series of equations or processes that can predict material losses but they are constraints at the application designed for and will be presented further. This study will assess FSW tool life prediction upon different material configurations, mainly steel grades as it impacts greatly the wear behavior of the tool.

EXPERIMENTAL PROCEDURE

Material properties

The material combinations used in this study has been determined under the NRC's ALTec industrial consortium which are presented in Table 1.

Table 1: Material combinations used in this study

Material combination identification	Upper aluminium sheet	Bottom steel substrate
1	1.6mm thick AA6082-T6	2.2mm thick AA1008 steel
2	1.6mm thick AA6082-T6	2.0mm thick DP800 galvanized steel
3	1.7mm thick AA5083 SPF	2.3mm thick 201LN stainless steel

As a reference, the aluminium alloys and steel grades mechanical properties and chemical composition are shown in Tables 2, 3 and 4. As it will be highlighted further in this paper, the temperature have a significant impact on these properties. When the tool spin in this materials, the temperature rise and make these properties no longer the same depending on the amount of heat generated by the combination of process

parameters. During this study, the change in yield stress for the steel grades were determined by *JMatPro* software® using the chemical composition of the steel to get the desired results in our case, the yield stress as function of the temperature.

Table 2: Mechanical properties for joining materials used in this study

Steel grades and Aluminium alloys	Load direction	Yield stress	Ultimate tensile stress	Elongation
		Mpa	Mpa	%
ASTM A1008	Tranverse	215	333	36,5
	Longitudinal	209	329.6	38
Stainless Steel 201LN	Transverse	572,3	819,9	45,6
	Longitudinal	531,8	911,8	54,3
DP800 hot-dipped gavanized	Transverse	585,1	943,2	14,6
	Longitudinal	548,8	922,7	15,1
AA6082-T6	Transverse	314,2	341,8	12,1
	Longitudinal	312,7	339,2	12,3
AA5083 SPF	Transverse	172,4	324,9	24,4
	Longitudinal	174,8	335,7	25,8

Table 3: Chemical composition of steel grades

Steel Grades	C	Si	Mn	Ni	Cr	Fe	Others
SS201LN	0,0336	0,4454	6,9783	4,5467	16,7711	70,2	bal.
DP800 Galvanized	0,147	0,2191	1,7927	0,02642	0,24	97,1	bal.
A1008	0,03	0,01862	0,2	Trace	0,0199	99,616	bal.

Table 4: Chemical composition of aluminium alloys

Aluminium Alloys	Si	Fe	Cu	Mn	Mg	Al	Others
AA5083 SPF	0,052	0,089	0,028	0,87	4,72	94	bal.
AA6082-T6	0,96	0,43	0,02	0,41	1,1	96,99	bal.

The transverse and longitudinal mechanical properties for the steel grades and aluminum alloys were obtained using a 25mm gage length extensometer under ASTM E8 standard. The first step in this study was to produce process windows for all the material configurations identify in Table 1. The second step was to determine a measurement methodology for FSW tool life evaluation and the last one was to correlate all the different parameters that can affect the tool wear resistance into an equation that predicts tool life. As it will be explained further in this paper, the initial microstructure of steel grades plays an important role in FSW tool wear results. The microstructures were obtained using a typical polishing sequence and different etchants were employed depending on steel grade to reveal grain boundaries (Figures 1 to 3).

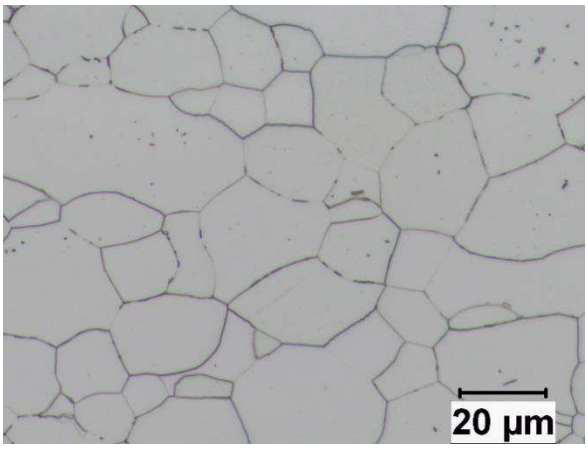

Figure 1: Microstructure of the steel ASTM A1008; *Nital* etchant

The figure 1 displays a fully ferritic microstructure which is typical of a low-carbon steel (1008). On the other hand, Figure 2 shows a mix between a ferritic and a martensitic microstructure as expected. Figure 3 shows an austenitic microstructure for the 201LN stainless steel and it is provided on the ¼ hard which indicates a certain amount of plastic deformation in the as-received state. This is corroborated by the high mechanical properties reported in Table 2.

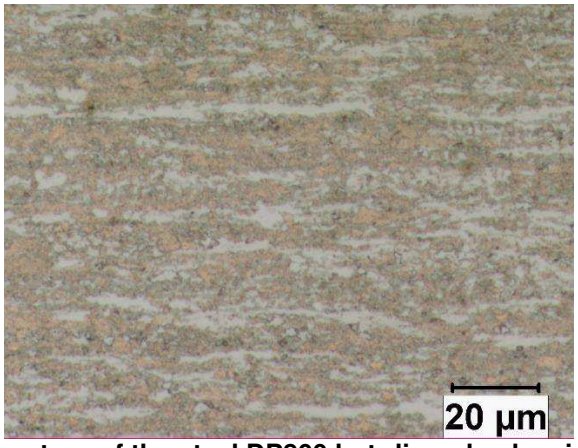

Figure 2: Microstructure of the steel DP800 hot-dipped galvanized; *Nital* etchant

Figure 3: Microstructure of the 201LN stainless steel; *Kallings* etchant

The Vicker's microhardness was also measured for each steel grade using an Akashi system coupled with a Clemex Vision camera at 150gf and the mean value over five indentations was given. For the 1008 steel and 201LN stainless steel, based on the mono-phase nature of the microstructure, the hardness was measured directly and shows 115HV and 287HV respectively. For the DP800 galvanized steel, given the dual-phase nature of the microstructure (ferrite and martensite), nano-indentation using an Anton Paar with a Berkovich indenter was provided at a force of 25mN. From figure 4, we can distinguish two distinct zones which refer to the ferrite and martensite phases. The Vicker's hardness is obtained from nano-indentation by a conversion equation that take account of the shape of our Berkovich indenter [6]. Applying this analysis, the highest values of hardness, representing martensite, reaches ≈600HV.

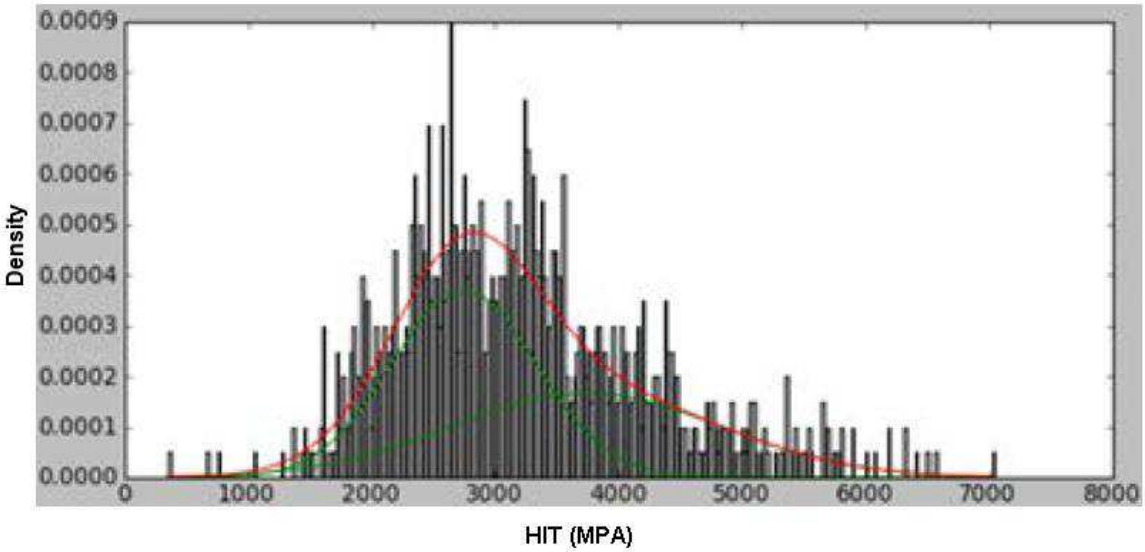

Figure 4: Hardness distribution done on a cross section of a sample of DP800 hot-dipped galvanized by Nano indentation

The friction stir welding was provided in lap joint configuration by a MTS I-Stir PDS system (figure 5 a) and b)).

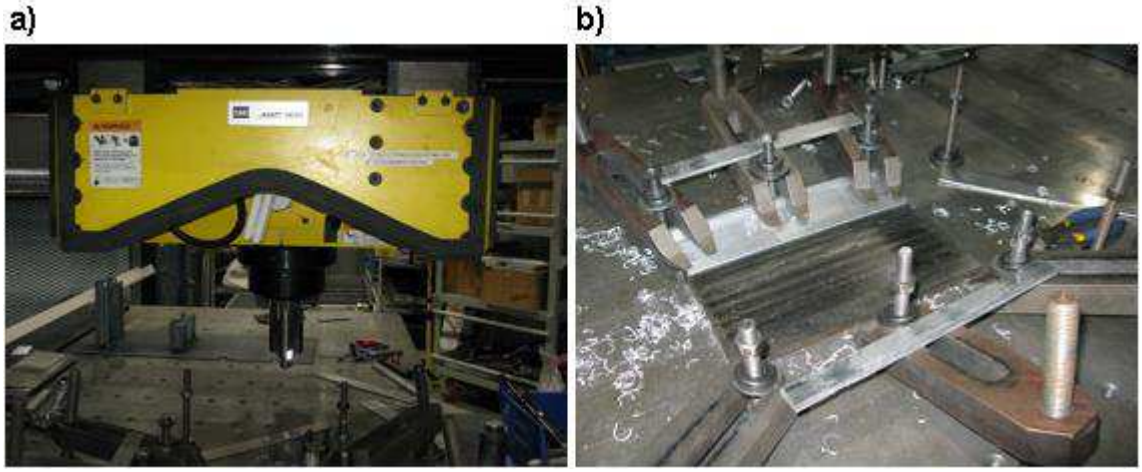

Figure 5: a) Head of the welder frame b) Clamps used to hold the plates in place

Welds were made on 300mm long coupons in position control first for each process parameters to being able to record the forge force and then in force control. Each FSW process parameters passed through visual inspection and microstructural analysis to

define the process window for each material configuration. The FSW pin tool design has a simple cylindrical shape and was made of WC-25%Co material (Figure 6).

Figure 6: FSW pin tool made of WC-25%Co

A microstructural analysis has been done on the FSW pin tool (Figure 7). It shows a wide distribution in size of hard WC particles into a cobalt binder. Although the size distribution of particles is not provided, this behavior could affect the wear rate of the FSW pin tool and will be discussed later. Temperature measurements have also been recorded as a thermocouple that was embedded in the shank of the FSW tool. It travels up to the root of the shoulder to identify the temperature variations between each FSW process parameters, thus heat input, in each material configuration (Figure 8).

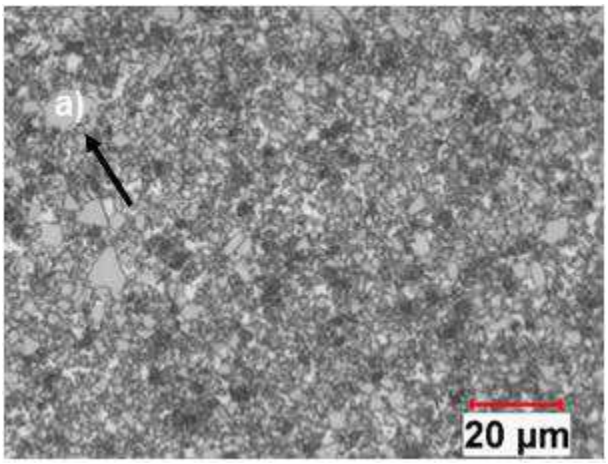

Figure 7: Microstructure of WC-25%Co; a) WC phase, light grey

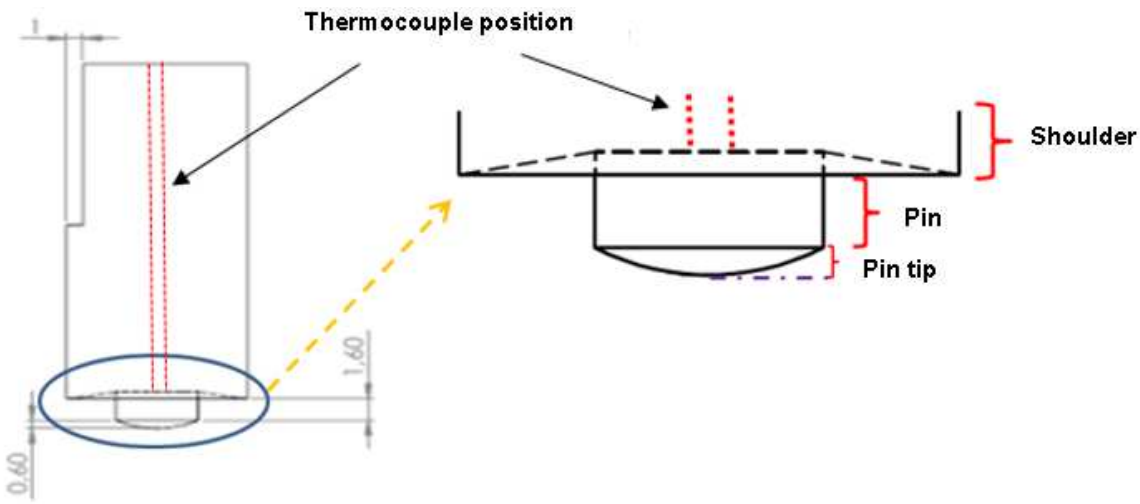

Figure 8: Schematic of thermocouple position in the FSW pin tool

For temperature readings, a grounded thermocouple of 0.5mm was inserted and connected using a wireless communication system to record in real time the temperature reached into the FSW pin tool at shoulder position. Although the thermocouple position do not indicate the exact local temperature at the aluminium-steel interface, this position is easier to monitor for production purpose and will be correlate ultimately with the mechanical properties.

FSW Tool wear measurements

The FSW tool wear was measured in 3D microtopography using a STIL system with a moving table and a fixed optic pencil (1µm precision) that read the height at constant steps (Figure 9). The results were then analyzed through *Mountain maps ®* software. The initial FSW tool tip profile was sketched first and the profile was taken again after distinct weld length as provided in Table 5. Some methods were tested to accurately acquire the wear of the tool, but the pin height was kept as the tracking parameter because of the steel adhesion on pin tip. It was easier to computationally erase the steel adhered on the surface of a cross section than do the same process with the whole surface of the pin tip.

Table 5: Analysis intervals between each scans of pin's tool by joining materials

Joining materials	Analysis intervals
AA5083 SPF/SS201LN	5
AA6082-T6/A1008	5
AA6082-T6/DP800	2

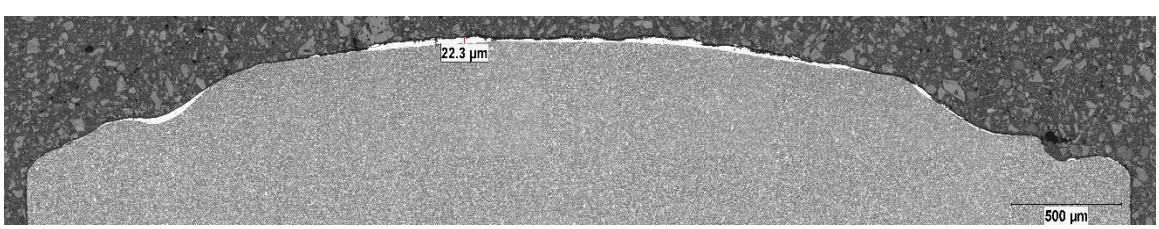

Figure 9: Cross section of a tool that show steel adhesion on pin tip (white surface layer)

Figure 10: 3D microtopography STIL system with the moving table and optic pencil

Once the FSW tool wear results were acquired, the last part of this study was the formulation of a tool life prediction. The FSW tool life is not a straightforward decision because it depends on how the end-user allowable, which can be related to the post-weld mechanical properties, the residual pin length or microstructural features such as the remained shear area, are determined. For the purpose of the present paper, a phenomenological law will be developed further regarding the pin length reduction over weld length, representing the FSW tool wear rate, disregarding the total tool life.

FSW tool wear rate models

In the FSW tool wear domain, the focus was done in the wear mechanisms which explains the type, and eventually, the conditions where wear takes place. Some works were done to investigate throughout all types of wear met in the FSW of steel. Two major works were taken seriously as they pointed out substantially the same wear mechanisms in roughly the same conditions of testing as ours. These works have target creep and intergranular failure of the microstructure as major causes but highlighted adhesive and abrasive wear were the main causes of the volume losses during the welding process [7-9].

The attractiveness for the aluminium alloys containing a certain amount of hard particles is gaining in popularity especially in the aeronautical and nuclear field due to interesting mechanical properties. Using FSW to join those materials causes some issue that some researcher worked on using H13 steel as FSW tool material. In fact, the tool have tendency to modify into a new specific shape which is optimized by itself when the joining materials are MMCs (Metal Matrix Composites). This phenomenon was highlighted first by a *R. A. Prado* [10]. Despite the tendency noted by the work just mentioned, no model or equation is presented that can predict the wear of the tool. However, the model of *Tracie J. Prater* [11] is well adapted for this purpose because the shape of the resulting tool and the conditions that work in show good similarities with the shapes presented in [10]. Equations are set to work with FSW in MMC in function of process parameters. According to the results of this work, the equation can predict the wear of the tool and show some good results at a certain level of precision. However, the conditions met in the papers aforementioned can be encountered only when the tool is totally embedded in the abrasive material namely, welds made in butt joint in MMC's.

Thus, this type of model can't described the conditions the tool works in this study but show us how flexible an equation based on process parameters can well fit the experimental results [12].

On the other hand, the simulation of friction stir welding take extents around the world these last years. Some authors have set new way to numerically predict tool wear with process parameters and get some good results [12]. However, these works previously mentioned used mainly Archard's wear law like constitutive equation. In [13], the formulation of a work made by Zmitrowicz was used in its simplest way :

$$\dot{d}_{wear} = \frac{k_{wear}}{H_v(T)A_c} \|\bar{F}_N\| \|\bar{v}_T\| \quad (1)$$

Where $\dot{d}_{wear}$ is the wear depth rate, k_{wear} is a material specific wear constant, $H_v(T)$ is the Vickers hardness of the tool affected by the temperature, A_c is the contact area between the tool and the interface, $\bar{F}_N$ is the normal force applied on the tool and $\bar{v}_T$ is the tangential speed of the tool where the wear is calculated.

Since the material specific wear constant k_{wear} is a coefficient found experimentally, it can be modified to fit the experimental results and units used in the equation. So, there are some models that can well predict the tool wear in FSW but no ones can be used in our conditions. A new equation that can predict the wear of the tool in FSW in lap joint in function of steel grades can be done properly by taking the formulation of Zmitrowicz and modified it to integrate the desired parameters. It will be developed further in this paper about the process that has been done to create this new equation based on equation 1.

RESULTS

FSW process window determination

To get the wear rate of a tool working in industrial environment, it is primary to perform the welds with process parameters that can be used in the assembly of real structures. For that, it is essential that the tool works in conditions met in this environment. The first step of this work was to achieve process window for each of the three combinations of the joining materials (figures 9, 10 and 11).

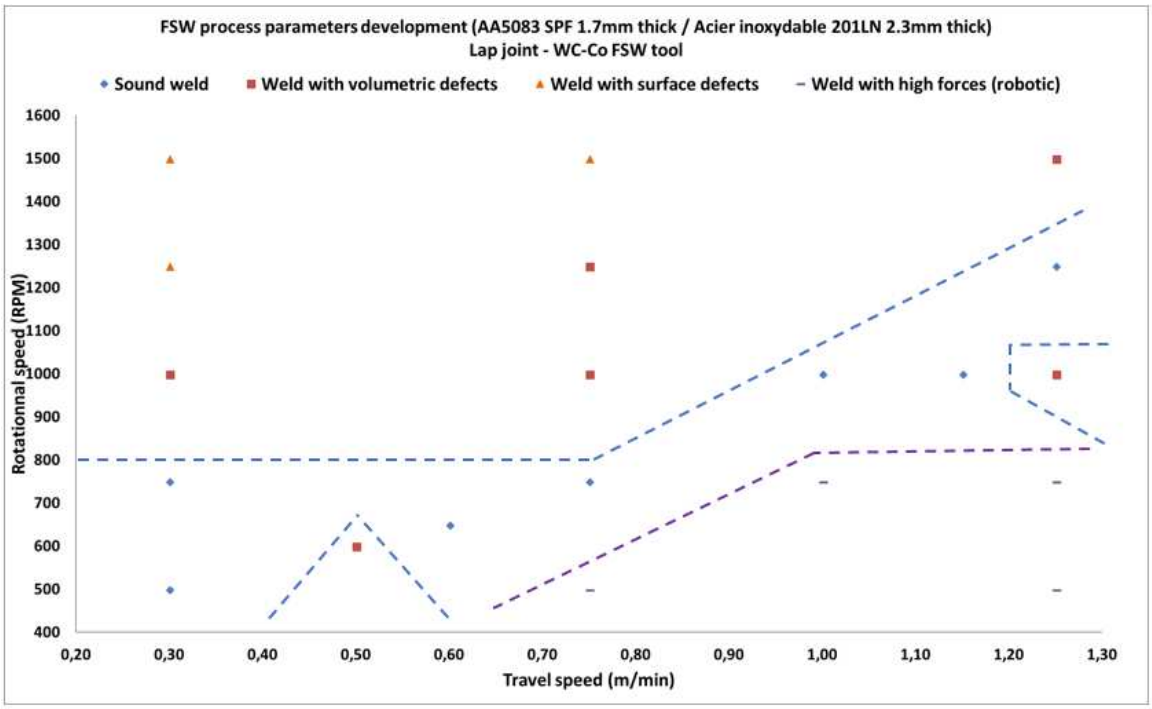

Figure 11: Process window for the assembly AA5083 SPF/SS201LN

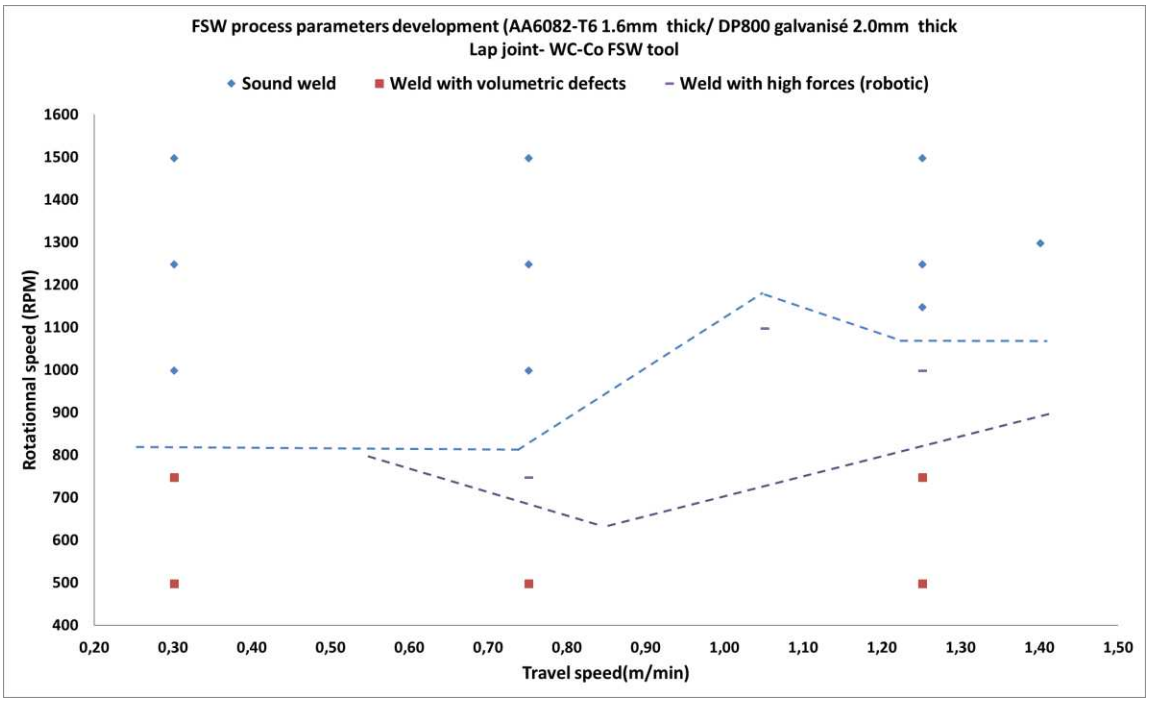

Figure 12: Process window for the assembly AA6082-T6/DP800 Galvanized

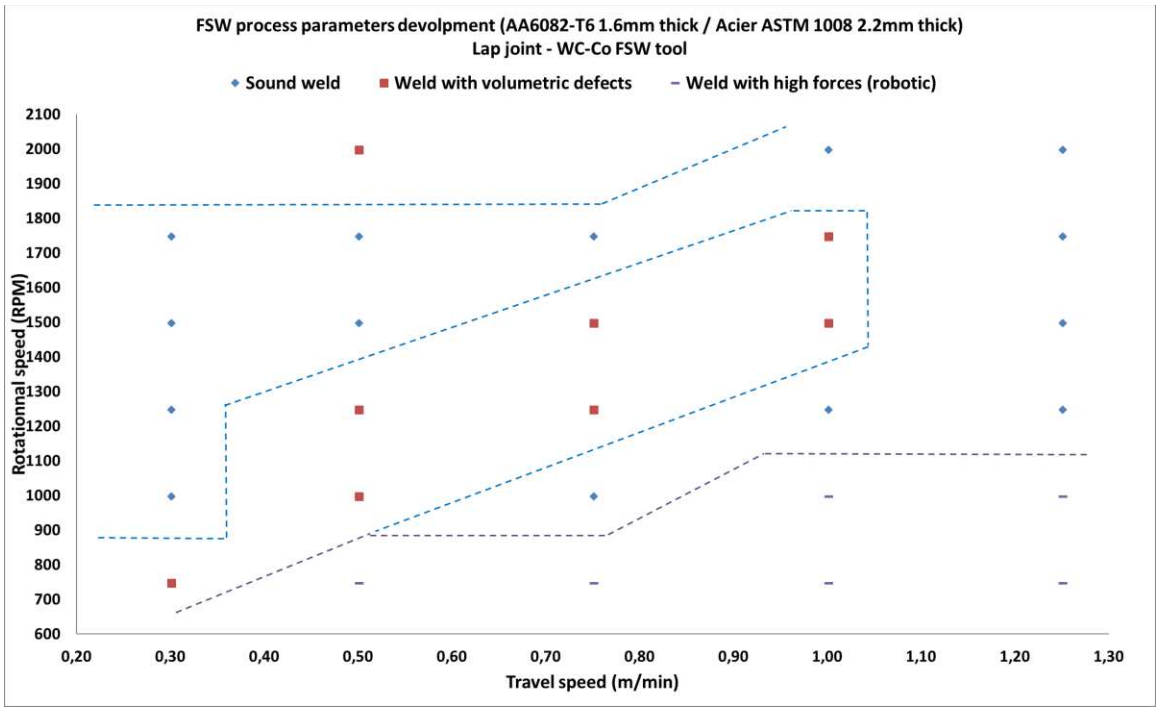

Figure 13: Process window for the assembly AA6082-T6/A1008

From figure 11, using a 201LN stainless steel as bottom sheet, it is observed that the formation of defects are promoted with higher rotational speed. This can be explained by the lower hardness of the steel, which is fully austenitic, as shown previously. With a high rotational speed, the tool tend to accentuate the steel ascent in the top sheet and thus, promote the formation of defects. This affirmation can be confirmed by the process window of the materials combination with DP800 as bottom sheet (figure 12). This steel shows a high hardness with a mixed microstructure (ferrite and martensite) and consequently do not promote defects at higher rotational speed as it does for the case previously mentioned. This joint seems to need a minimum of 1000 RPM to generate sound welds. From figure 13, using A1008 steel as bottom sheet, the process window is more critical as predetermined revolutionary pitches need to be targeted to avoid defect formation. This steel is very easily deformed which indicates a carefulness in the chosen parameters to avoid potential defects, mainly disrupted steel remnants in the nugget zone (Figure XX).

From these process window, the combinations of process parameters must be selected between these ones that give sound welds for each material configuration for wear experiments. The next section will give a sketch of the tool temperature and will help to understand the selection of the combinations of process parameters. For the assembly using SS201LN as bottom sheet, the revolutionary pitch was kept at 1.0 mm/revolution which promote a decent travel speed that could be usable in production. From the process window presented on the figure 10, 0.75 m/min with 750 RPM and 1.25 m/min with 1250 RPM were chosen. For the assembly using DP800 galvanized as bottom sheet presented on the figure 11, 1.25 m/min with 1250 RPM was taken. For the assembly using A1008 steel as bottom sheet, 1.0 m/min with 2000 RPM was used for the wear experiments. Each of the combinations of parameters have the proper forge force previously evaluated.

FSW tool temperature analysis

Because of the large amount of the material needed to completely assess the whole spectrum of the process parameters, only a complete analysis was done with the joint using A1008 steel. The figures 14 to 18 gives the temperature in degree Celsius in function of the rotational speed for each of the key travel speed used in this study. Some large offset of the regression line can be seen and it is probably due to the forge force applied. As known, a higher forge force is required to produce sound weld but the force interval is large depending on the bottom sheet. A difference of 2.5 to 3.0kN can produce the same weld without any visible difference but give different temperature. The stick-slip phenomena can explain this observation by changing the friction condition between the stick and the slip condition around the forge force employed [14].

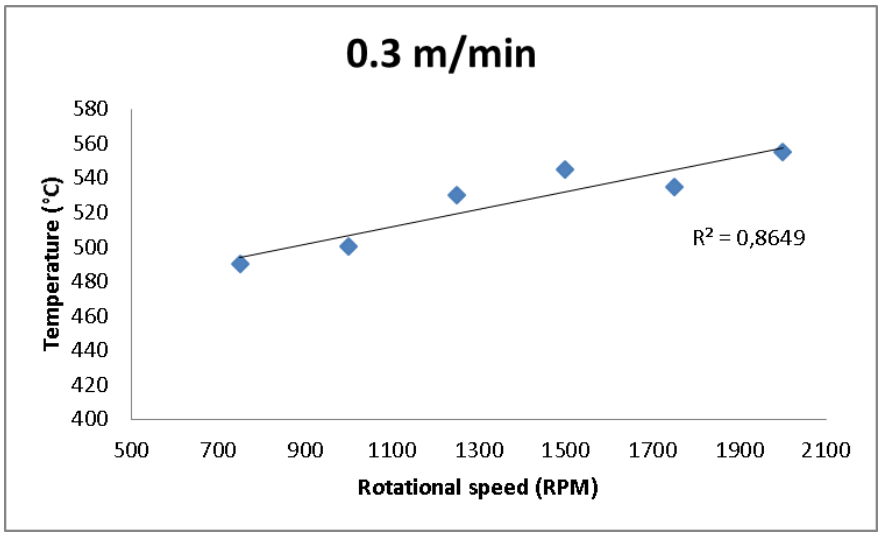

Figure 14: Temperature in function of rotational speed for 0.3 m/min (A1008)

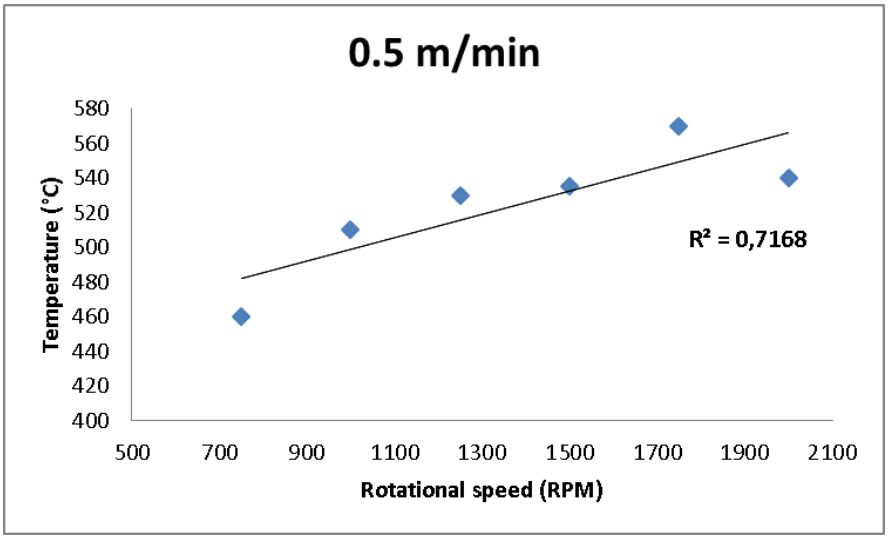

Figure 15: Temperature in function of rotational speed for 0.5 m/min (A1008)

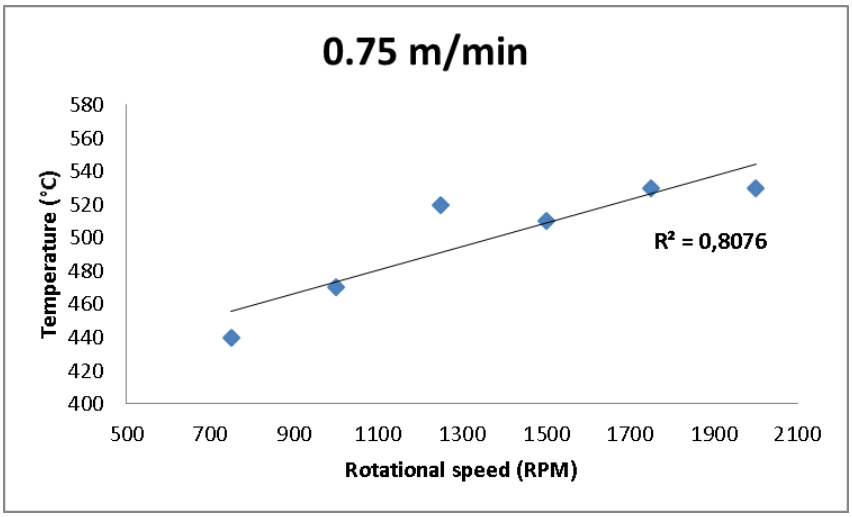

Figure 16: Temperature in function of rotational speed for 0.75 m/min (A1008)

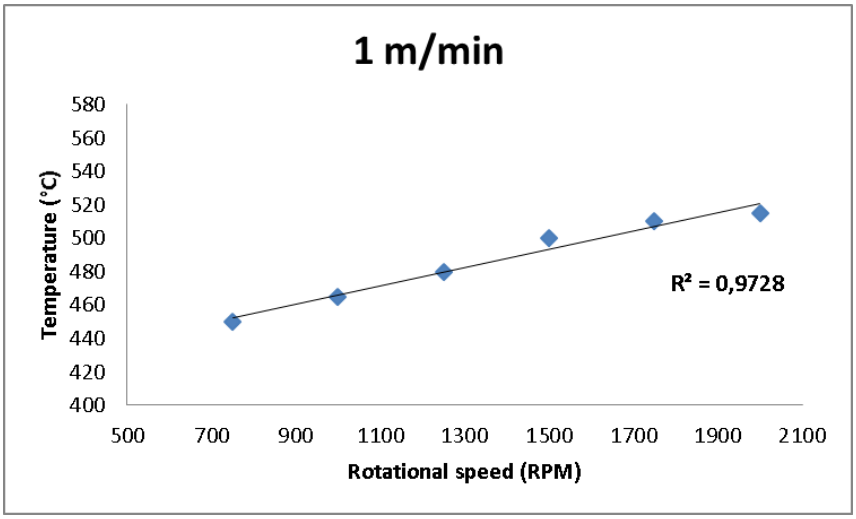

Figure 17: Temperature in function of rotational speed for 1.0 m/min (A1008)

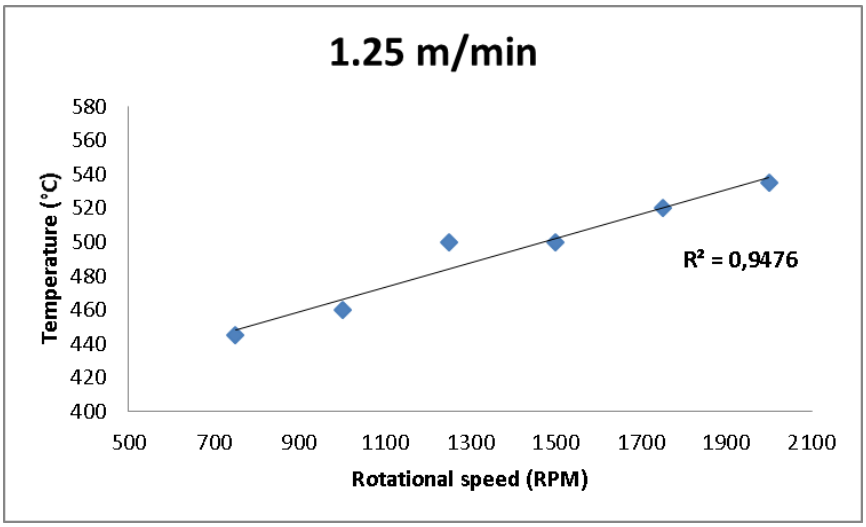

Figure 18: Temperature in function of rotational speed for 1.25 m/min (A1008)

FSW tool wear rate

Figures 19 to 22 are the results of the wear welds according to table 5. Some of the analysis by microtopography was unusable due to undefined shape of the tool in comparison of the sticking of steel on the tip of the pin.

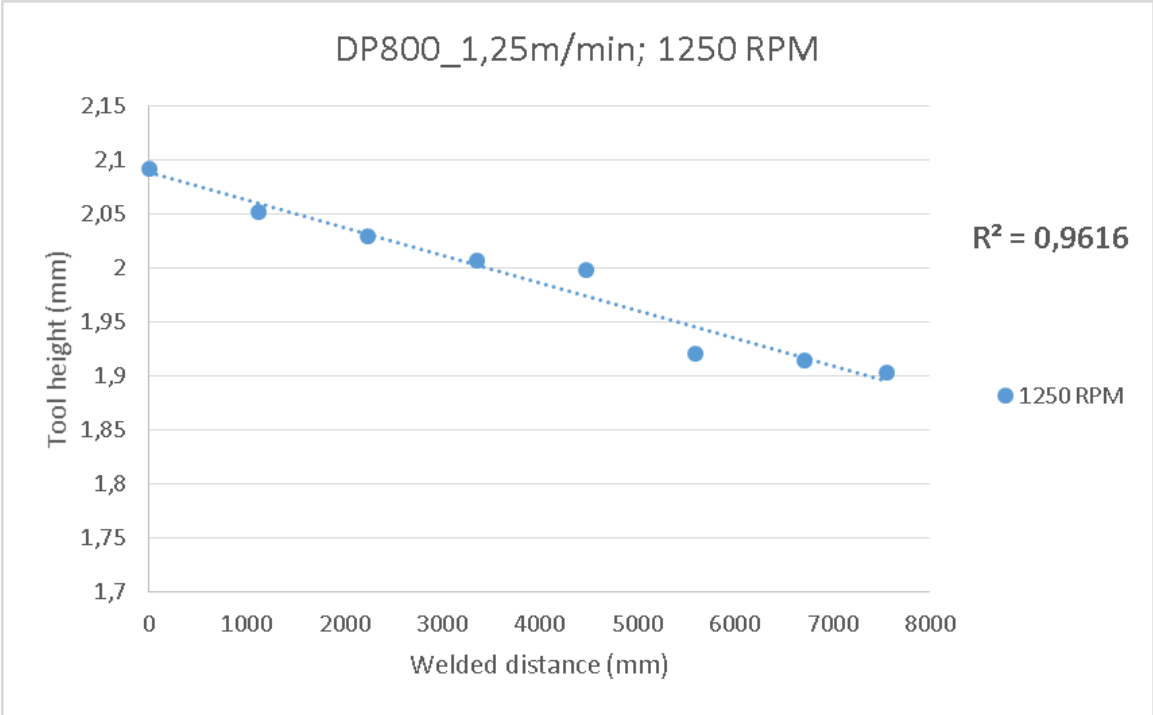

Figure 19: Tool height in function of welded distance in DP800's assembly at 1.25 m/min; 1250 RPM; 18 KN

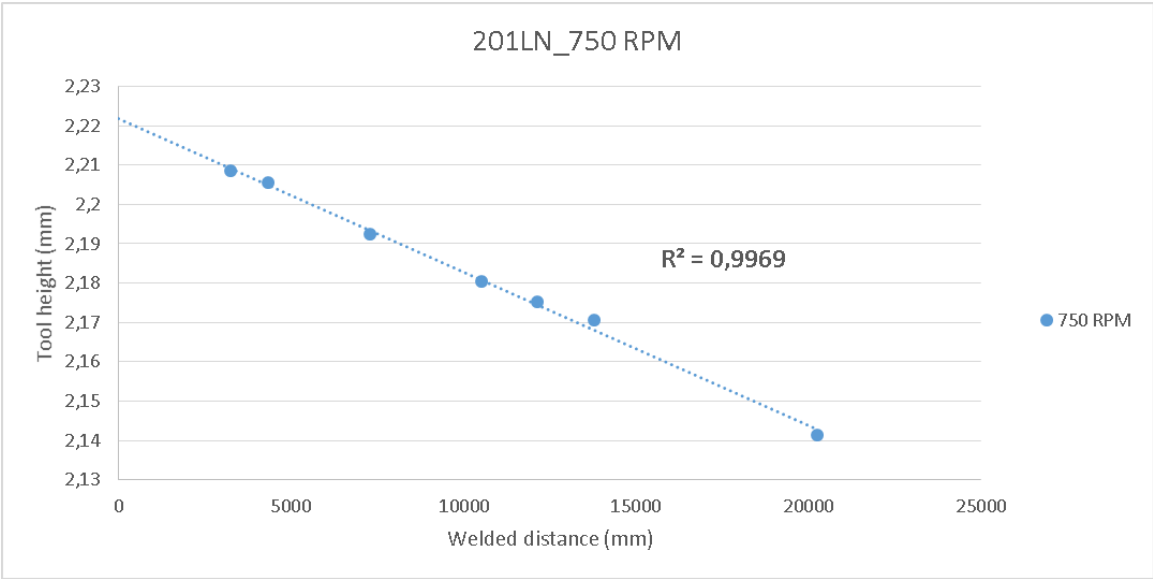

Figure 20: Tool height in function of welded distance in SS201LN's assembly at 0.75 m/min; 750 RPM; 16 KN

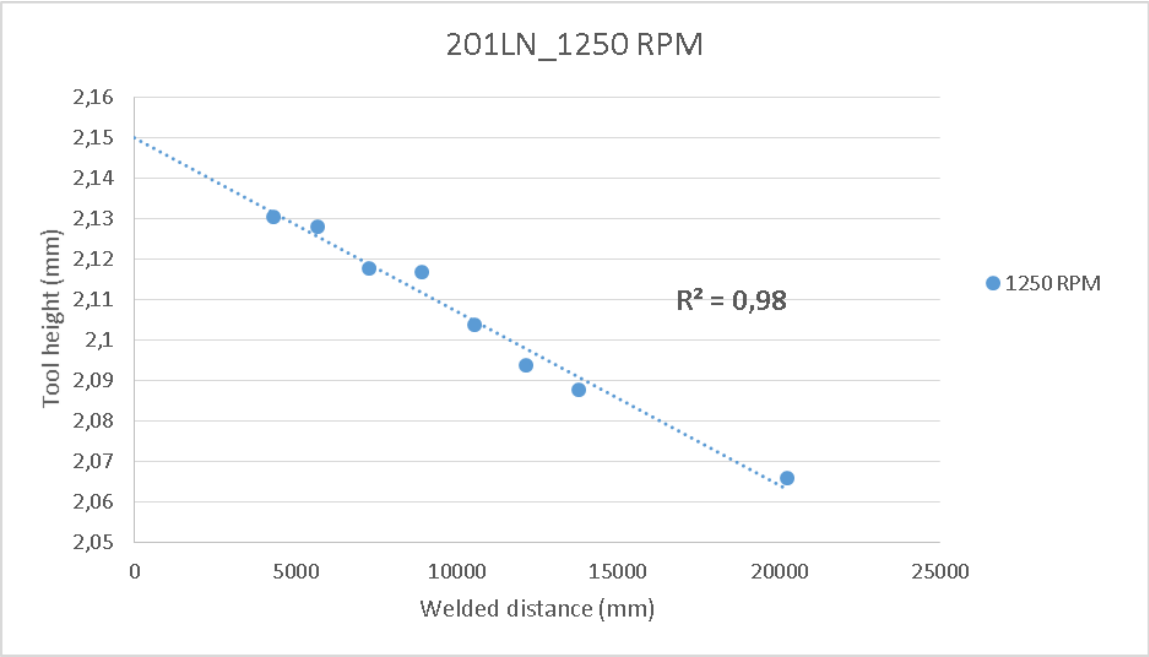

Figure 21: Tool height in function of welded distance in SS201LN's assembly at 1.25 m/min; 1250 RPM; 17 KN

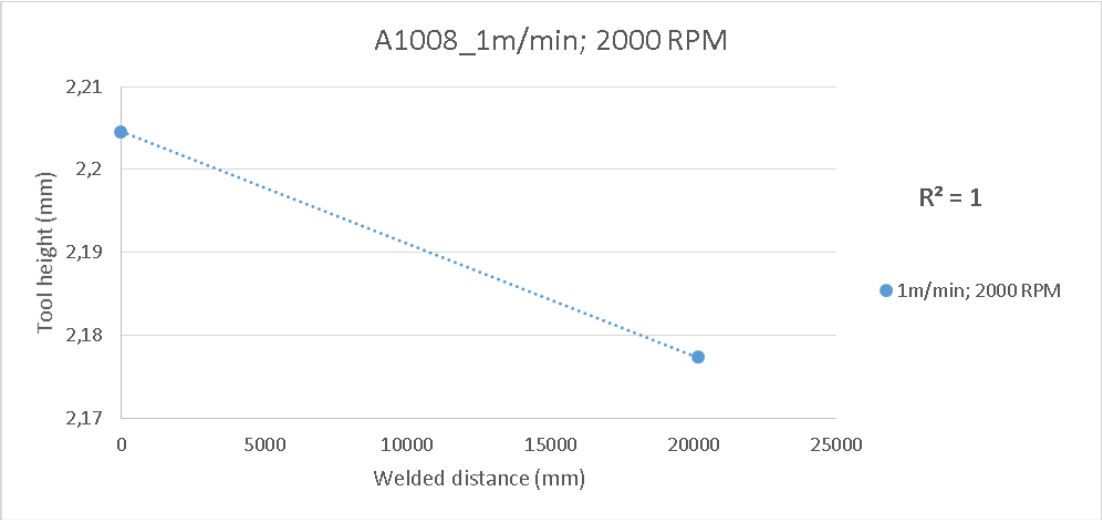

Figure 22: Tool height in function of welded distance in A1008's assembly at 1 m/min; 2000 RPM; 6.5 KN

Each of the set of wear results express a linear tendency depending on process parameters and steel grades. The wear rate for each of them were calculated by taking the gradient of the slope done by the regression line. The wear rate is dependant of how the tool was measured, so the units of those ones are given in mm of loss in tool height by mm of weld. The figure 19 gives $2.50437X10^{-05}$ in DP800 galvanized steel using 1250 RPM at 1.25 m/min with 18 KN. The figure 20 and 21 can give the wear rate for the two conditions tested in 201LN stainless steel, 750 RPM at 0.75 m/min with 16 KN of forge force and 1250 RPM at 1.25 m/min with 17 KN. Respectively, the wear rate are $3.97185X10^{-06}$ and $4.15309X10^{-06}$. For the case using low-carbon steel 1008, the wear rate is $1.35218X10^{-06}$ using 2000 RPM at 1.0 m/min with 6.5 KN. These results confirms that the microstructure have a major impact on the wear rate. For the rotational speed

and the travel speed, the wear rate in the DP800 is about 6 time greater than the wear rate for the second combination of process parameters in 201LN and only 1 KN of difference in forge force. The dual-phase steel have a hardness of about 2 time greater the hardness of the stainless steel used in this study.

As mentioned earlier, the pin height was taken to be the tracked parameters due to sticking of steel on the pin tip and it was impossible to take it out without damaging the tool itself. On the other hand, the pin height does not reflect the whole wear of the tool because it does not take account of edges losses.

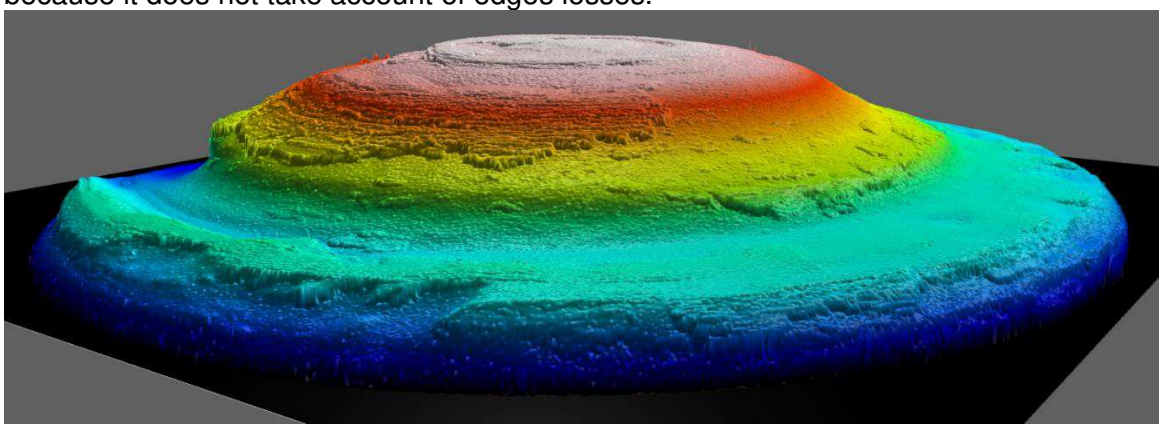

Figure 23: Computer reconstruction of pin tip by Mountains Map of the tool used for wear welds after 20 meters

DISCUSSION

Following the data collected, an analysis must be done on the parameters that affects the tool wear. Equation 1 is taken and shelled into its respective parameters. Each of them are take apart and check if there is any impact on the mechanical properties that can affect significantly the wear of the tool.

$$\dot{d}_{wear} = \frac{k_{wear}}{H_v(T)A_c} \|\bar{F}_N\| \|\bar{v}_T\|$$

Because the measure are taken on the tool, the first thing to analyze is the effect of the heat on the hardness of the tool and the contact area. After the wear tests have been completed, the hardness of the tool was taken near the tip of the tool and far away from the pin tip and the shoulder to ensure that the heat did not affected the material. The results was quiet similar and done a Vickers hardness of about 980. For the real contact area, it was determined using the software mentioned above.

As far as the coefficient $\dot{d}_{wear}$ give a number in volume (mm^3) over distance of welding (mm), it was needed to modify this one and do have a coefficient that gives a value in height of the tool (mm) by welded distance (mm). It will be called W_r. The tangential speed $\bar{v}_T$ is no longer needed in the new formulation given that the speed parameter must represent the whole tool and not a precise point on the tool. To represent the number of time that the tool scrubbed on the steel by millimetre of advance, the inverse revolutionary pitch $\frac{\omega}{v}$ (rev. /mm) is used. For the applied normal force $\bar{F}_N$, it stays like that because it quantify the pressure of the pin tip.

The coefficient k_{wear} will be no longer used since it does not fit with the new formulation. It is replaced by three different parameters that express better how the variation in the steel grades affect the wear rate. First, it is essential that the reduction of mechanical properties in function of temperature must be considered in the range of operational temperature. Thus, a ratio of reduction in yield limit between 500°C and 600°C for the steel was used called f_B which is the behavior factor express as a ratio of strain rates commonly found in simulations [15]. After that, the effect of the hardest phase of the studied steel must take in account. For that, the Vicker's hardness of that phase (HV_h) and the percentage in volume were introduce in this formulation. After that, a coefficient was created (k_g) to balance and to fit the reference material.

$$W_r = \frac{HV_h\left(\frac{1}{(1-\%v\ HV_h)^n}\right)\left(\frac{\sigma_y\ 100\ s^{-1}}{\sigma_y\ 1\ s^{-1}}\right)k_g}{(H_{vo} * A_{cr})}\|\bar{F}_N\|\left(\frac{1}{f_M}\right)\left(\frac{\omega}{v}\right) \tag{2}$$

The equation 2 is the new formulation that can predict the wear of the tool in function of steel grades by the composition of the microstructure and their behavior in FSW process.

$$W_r = \frac{HV_h C_M f_B k_g}{(H_{vo} * A_{cr})}\|\bar{F}_N\|\left(\frac{1}{f_M}\right)\left(\frac{\omega}{v}\right) \tag{3}$$

The equation 3 is the compact form of the equation 2 and it is easier to understand what the purpose of all of this coefficient when the meaning is known, that is why the new form will be commonly found like the equation 3.

The methodology adopted was to set the phenomenological equation on a reference material to make sure that fit at least one case and set it like a starting point. This material was the DP800 and has shown the highest amount of wear of the tool height. Afterward, the wear of the pin height in the other joining materials are compared to this reference case. This is how the wear rate of the pin height is obtained for each case.

The mechanism factor f_M is specific to the dominant wear mechanism encountered during the welding of the studied steel. Wear mechanisms seen in this type of application were raised by authors who focused only on wear mechanisms of FSW in steel. These ones were taken as cited in the mentioned references [7], but the values of the mechanism factor were found by setting the roughest wear mechanism as 1 (abrasion) and deduced the value of the adhesion wear mechanism. The way used to deduce this value is simply by trying to get a unique value that fit as good as possible for the other three cases of this study.

The microstructure coefficient varying depend on if the material is single or dual phase. If the material is single phase n will have a value of 0. If the material is dual phase, the value of n will be 1 to consider the percentage in volume of the hardest phase of this material has a greater impact on the wear rate. H_{vo}, the hardness of the tool remains the same throughout the experiments (980 HV).

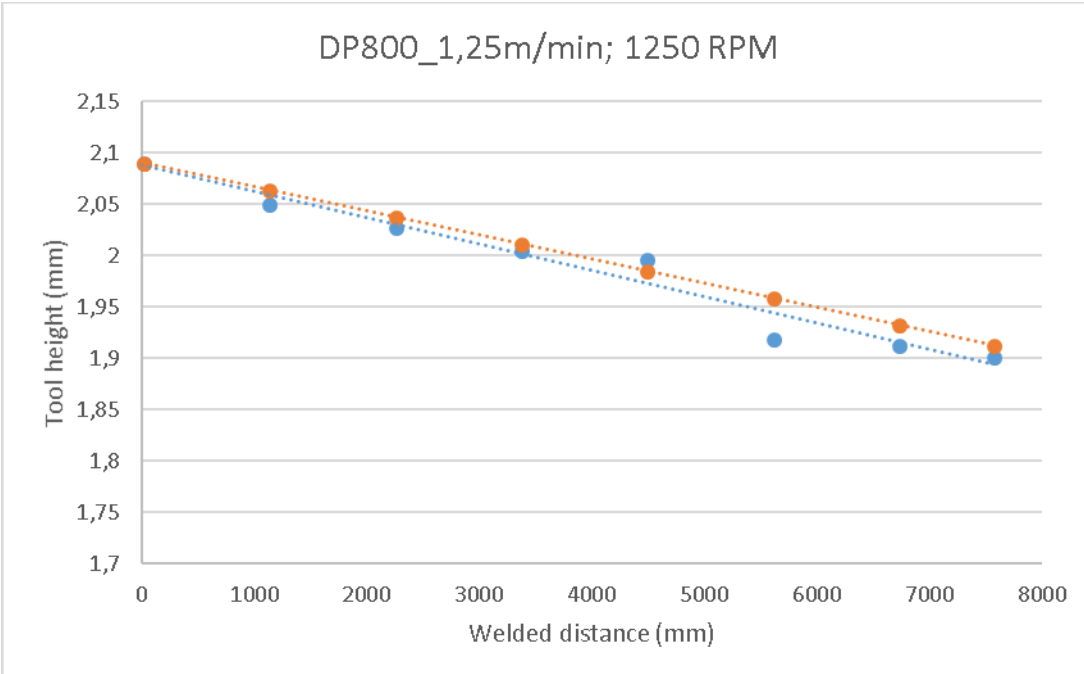

Figure 24: Experimental tool height and calculated tool height by the phenomenological equation in DP800's assembly

Table 6: Results of calculated wear rates an error % with the experimental wear rates

Joining materials	Process parameters	Experimental wear rates	Calculated wear rates	Error % on wear rates
ASTM A1008	1 m/min; 2000 RPM; 6,5 KN	1,35218254E-06	1,50990035E-06	11,66
Galvanized DP800	1,25 m/min; 1250 RPM; 18 KN	2,50436508E-05	2,50436507E-05	0,00
201LN stainless steel	0,75 m/min; 750 RPM; 16 KN	3,97185185E-06	3,93988624E-06	0,80
	1,25 m/min; 1250 RPM; 17 KN	4,15308642E-06	4,17546201E-06	0,54

A phenomenological equation was developed with the parameters that have a significant impact on wear. Those parameters are the process parameters, the steel grades and the tool material. With this equation, wear rates were calculated for the three combinations of joining materials. 4 cases were tested for wear trials as shown in table 6 and three of them have good percentage between the experimental and calculated wear rates. However, only one case have much more error percentage than the other.

CONCLUSION

In this paper, the process of predicting the wear of tools used in friction stir welding in lap joint configuration of aluminum and steel was analyzed. Three steel grades, with different microstructures, were used to characterize its behavior on the wear rate. The steel that shows the highest wear rate is the reference material for the equation. The other two steel grades were used to validate the wear model. The main observations of this study are:

- The steel grades shows a different behavior on the process window definition. The change in hardness appears to be the major factor contributing the difference observed as a low hardness promotes a higher steel reminiscence in the nugget zone.

- The rotational speed has a direct impact on the FSW tool temperature, which was expected.

- The Zmitrowicz version of the Archard's wear law was the initial determined model to this study. Per this equation, a modified one, which takes account of the steel grade's microstructure, the process parameters and the FSW tool material was developed which shows a good prediction when it comes down to the wear rate depending on steel grades.

- The same way to find the wear factors for each case in this study were used by *J. F. Archard* to get the wear factor for each material in tribology which are used in handbook for conception [16].

- The phenomenological equation developed in this study gave good results for the materials combinations tested.

REFERENCES

[1] S. Rajaram, "Welding equipment and supplies: The global market - focus on solid state welding," 2014.

[2] D. J. Spinella, "Common joining metghods used in aluminum structures," ed: Alcoa, 2013.

[3] T. Curtis, C. Widener, M. West, B. Jasthi, Y. Hovanski, B. Carlson*, et al.*, "Friction stir scribe welding of dissimilar aluminum to steel lap joints," *The minerals, metals & materials society,* vol. Friction stir welding and proceeding VIII, pp. 163-169, 2015.

[4] A. A. M. d. Silva, E. Aldanondo, P. Alvarez, E. Arruti, and A. Echeverria, "Friction stir spot welding of AA 1050 Al alloy and hot stamped boron steel (22MnB5)," *Science and Technology of welding and joining,* vol. 15, pp. 682-687, 2010.

[5] O. S., "Application of an FSW continuous welding technology for steel and aluminum to an automotive subframe," 2013.

[6] T. Sawa, "Correlation between nanoindentation test result and Vickers hardness," presented at the Metrology in modern context, Thailand, 2010.

[7] M. Eff, "The effect of tool texture on tool wear in friction stir welding of X-70 steel," Master of science, Welding engineering, The Ohio state University, 2012.

[8] J. Wang, J. Su, R. S. Mishra, R. Xu, and J. A. Baumann, "Tool wear mechanisms in friction stir welding of Ti–6Al–4V alloy," *Wear,* vol. 321, pp. 25-32, 2014/12/30/ 2014.

[9] B. T. a. S. S. Babu, "Tool degradation characterization in the friction stir welding," vol. 89, 2010.

[10] R. A. Prado, L. E. Murr, K. F. Soto, and J. C. McClure, "Self-optimization in tool wear for friction-stir welding of Al 6061+20% Al2O3 MMC," *Materials Science and Engineering: A,* vol. 349, pp. 156-165, 2003/05/25/ 2003.

[11] T. J. Prater, A. M. Strauss, G. E. Cook, B. T. Gibson, and C. D. Cox, "A phenomenological model for tool wear in friction stir welding of metal matrix composites," *Metallurgical and materials transactions A,* vol. 44A, 2013.

[12] B. Gibson, G. Cook, T. Prater, W. Longhurst, A. M. Strauss, and C. D. Cox, "Adaptive torque control of friction stir welding for the puspose of estimating tool wear," *Journal of engineering manufacture,* vol. 225, pp. 1293-1303, 2010.

[13] A. Zmitrowicz, "Wear patterns and laws of wear - A review," *Journal of theoretical and applied mechanics,* 2006.

[14] M. A. Waheed, L. O. Jayesimi, S. O. Ismail, and O. U. Dairo, "Modeling of heat generations for different tool profiles in friction stir welding: study of tool geometry and contact conditions," *Journal of applied and computational mechanics,* vol. 3, p. 23, 2017.

[15] A. Arora, Z. Zhang, A. De, and T. DebRoy, "Strains and strain rates during friction stir welding," *Scripta Materialia,* vol. 61, pp. 863-863, 2009.

[16] J. F. Archard, "Contact and rubbing of flat surfaces," *journal of applied physics,* vol. 24, pp. 981-988, 1953.